A Nonintrusive Magnetically Self-powered Vibration Sensor for Automated Condition Monitoring of Electromechanical Machines

Jinyeong Moon, Peter Lindahl, John Donnal, and Steven Leeb
Massachusetts Institute of Technology
Cambridge, Massachusetts 02139
Email: jinmoon@mit.edu

Lt. Ryan Zachar
U.S. Navy
Bath, ME 04530

Lt. William Cotta
U.S. Coast Guard
Washington, DC 20593

Christopher Schantz
Infratek Solutions
Princeton Junction, NJ 08550

***Abstract*—This paper presents a nonintrusive and electromagnetically self-powered embedded system with vibration sensor for condition monitoring of electromechanical machinery. This system can be installed inside the terminal block of a motor or generator and supports wireless communication for transferring data to a mobile device or computer for subsequent performance analysis. As an initial application, the sensor package is configured for automated condition monitoring of resiliently mounted machines. Upon detecting a spin-down event, e.g. a motor turn-off, the system collects and transmits vibration and residual back-emf data as the rotor decreases in rotational speed. This data is then processed to generate an empirical vibrational transfer function (eVTF) rich in condition information for detecting and differentiating machinery and vibrational mount pathologies. The utility of this system is demonstrated via lab-based tests of a resiliently mounted 1.1 kW three-phase induction motor, with results showcasing the usefulness of the embedded system for condition monitoring.**

I. Introduction

Condition-based maintenance (CBM) is the maintenance of equipment when performance indicators show the occurrence of system degradation. Compared to run-to-failure maintenance, which is performed only after failure occurs, or routine-based maintenance where maintenance is scheduled periodically regardless of system health, condition-based maintenance provides several advantages [1]–[3].

For the U.S. Armed Forces, these advantages include improved safety and security, and increased operational availability of systems, as high-consequence failures are avoided. Further, CBM can reduce operational cost as maintenance labor and use of replacement parts are minimized. For these reasons, the Department of Defense (DoD) recently established their Condition Based Maintenance Plus (CBM^+) [4] strategy for better sustaining DoD systems. Implementing CBM, however, requires installing condition-monitoring sensors in machinery to capture real-time data, and developing analysis techniques to convert data into performance metrics and actionable knowledge for an operator.

This paper presents a nonintrusive and self-powered embedded system and an associated performance analysis method for condition monitoring of electromechanical machinery. This embedded system is designed for installation inside the terminal block of a typical motor or generator and harvests power from the magnetic field emanating from a current-carrying wire of the electromechanical load under monitoring [5], [6]. The energy harvester powers the sensor package, consisted of low-power microcontrollers and sensors, e.g. a 3-axis accelerometer, a temperature sensor, and a non-contact back-EMF sensor. Additionally, the system supports wireless communication for transferring data from the installed embedded system to operator's mobile devices or computer for signal-processing and performance analysis [7].

For an initial case study, the self-powered embedded system is configured for automated condition monitoring of resiliently mounted machines, e.g. generators and motors aboard Navy and Coast Guard ships. The power electronic circuits inside the energy harvester nonintrusively detects the start of a machine's spin-down, e.g. when a seawater pump turns off, via an abrupt change in current in the machine's power wiring. The vibration and back-EMF voltage data before and after the spin-down within a pre-specified window are automatically recorded. This data is then transmitted to a user device, e.g., a tablet or a nearby server, and processed to estimate the speed of the rotor as it slows down from steady-state operation to standstill. The vibration data and the estimated speed are then signal-processed to generate an empirical vibrational transfer function (eVTF) [8]. This transfer function is rich in condition information for detecting and differentiating not only machinery pathologies, but also problems with vibrational mounts.

The performance of this non-intrusive self-powered embedded system is demonstrated on a lab-based 1.5 hp (1.1 kW) three-phase induction motor drive system with a resiliently mounted baseplate similar to those used on machinery aboard Naval ships. Results from these tests match well with tests conducted using conventional accelerometer systems, and data collected using this system are processed to reveal condition indicators regarding both machinery imbalance and mount degradation.

978-1-5090-0790-5/16/$31.00 ©2016 IEEE

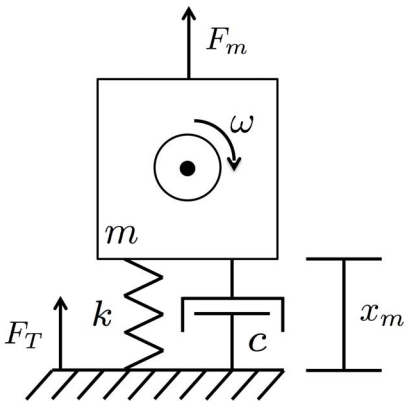

Fig. 1. 1-D Free body diagram for electromechanical machinery and mount system.

II. Vibrational Transfer Function (VTF)

An electric motor or generator mounted on resilient mounts is often modeled as a spring-mass-damper system with an eccentric mass vibration [9], as depicted in Fig. 1.

Here, the motion of the actuator mass is governed by the equation,

$$m\ddot{x}_m(t) + c\dot{x}_m(t) + kx_m(t) = F_m(t), \tag{1}$$

where m is mass, x_m is the position of the system, k is the spring constant, c is the damping ratio associated with the mount, t is time, and $F_m(t)$ is a forcing function. With acceleration the 2nd time-derivative of position, the Laplace-domain relationship between acceleration, $A_m(s)$, and the system forcing, $F_m(s)$, is derived from (1) as

$$\frac{A_m(s)}{F_m(s)} = \frac{\frac{s^2}{m}}{s^2 + \frac{c}{m}s + \frac{k}{m}} \tag{2}$$

where s is the Laplace transform operator.

Under steady-state conditions, the system forcing along the x-direction takes the form

$$F_m(t) = C\omega_m^2 \cos(\omega_m t) \tag{3}$$

where C is a constant related to load mass and imbalances, and ω_m is the speed of the rotating shaft. By defining a proportionally related "virtual input" function as

$$\Phi_m(t) = \omega_m^2 \cos(\omega_m t) \tag{4}$$

and substituting its corresponding Laplace representation into (2) to get

$$\frac{A_m(s)}{\Phi_m(s)} = \frac{C\frac{s^2}{m}}{s^2 + \frac{c}{m}s + \frac{k}{m}}, \tag{5}$$

we achieve a transfer function with the same dynamic properties, e.g. natural frequency, as (2), but one which also scales as the forcing coefficient, C, changes, e.g. due to an increased load imbalance. This is the equation we refer to as the vibration transfer function (VTF).

An empirical representation of this transfer function or "eVTF" can be achieved opportunistically with an installed self-powered embedded system. That is, during a motor or generator spin-down, i.e. a turn off event, the rotor speed and thus the eccentric vibration decreases from the steady-state operating speed to stand-still. The onboard vibration and back-emf sensors can collect operational data during this period, and the wireless transmitter can send it to a computer for eVTF processing. As explained below, the properties of this eVTF can then be used for CBM.

CBM Application: Machine Radiated Noise

In many situations, the force transmitted from the machine to the surface underneath, F_T (Fig. 1) is a major concern. For example, a Navy ship may need to maintain its radiated acoustic noise at a minimum to avoid detection, and an increase in force transmitted from the machine can lead to increased noise levels. Unfortunately, directly measuring such transmitted vibrations is difficult. Instead, performance metrics available from the eVTF can be used for estimating changes in F_T relative to a normalized value when the transmitted force is known to be acceptable.

In steady-state, an electromechanical machine has a transmissibility in the isolation range that is similar to that for zero damping. Therefore, c can be ignored as long as the operating speed is away from resonance [10], [11]. This means the force transmitted through the mounts to the baseplate occurs primarily through the stiffness of the mounting (the spring in Fig. 1), and follows Hooke's law,

$$F_T(t) \approx k \cdot x_m(t). \tag{6}$$

From (5), the natural frequency of the 2nd order system representation is related to the spring constant by $\omega_n^2 = k/m$. For eccentric mass excitation, the system acceleration follows simple harmonic motion, i.e. $a_m(t) = A_{m,ss}\cos(\omega_{ss}t)$, where the ss denotes steady state conditions. Substituting these relationships into (6) reveals

$$F_T(t) = -\frac{m\omega_n^2 a_m(t)}{\omega_{ss}^2}. \tag{7}$$

Typically for diagnostic purposes, only the magnitude of F_T is of concern; taking the magnitude of (7) yields,

$$|F_T| = \frac{m\omega_n^2 A_{m,ss}}{\omega_{ss}^2}, \tag{8}$$

where A_m is the magnitude of the acceleration. In many situations, the system mass, m, and the machine's steady-state operating speed, ω_{ss}, are consistent whenever the machine is in normal operation. As such, an estimate of the ratio of force transmissions from a time when the machine is in a known "good" condition, $|F_T|$, to the present condition, $|F_T|'$, can be achieved from only acceleration and speed measurements of the motor, i.e.

$$\frac{|F_T|'}{|F_T|} = \frac{\omega_n'^2 A'_{m,ss}}{\omega_n^2 A_{m,ss}}. \tag{9}$$

Here, ω_n^2 and $A_{m,ss}$ are values from when the machine is in the "good" condition and $\omega_n'^2$, and $A'_{m,ss}$ are derived from the most recent measurements. Practically, (9) indicates the value of estimating the eVTF for (5) during machine spin-down. From the eVTF, it is possible to estimate the transfer function peak or, essentially the natural frequency of the system from the observed resonant peak. Estimation of the natural frequency of the mount from the eVTF makes it possible to distinguish machine imbalance from degradation of the mount, both conditions which can cause increased transmitted vibration that might be indistinguishable from steady-state measurements alone. Changes in the forcing function, e.g. the vibration energy created by operating the machine, will generally increase the magnitude of the entire eVTF. Aging or degradation of the mount alone will shift the resonant frequency of the eVTF. Comparison of successively observed eVTFs can be used to distinguish progressive imbalance from aging of the mount.

III. The Self-powered Embedded System

The self-powered embedded system is called VAMPIRE: vibration assessment monitoring point with integrated recovery of energy. VAMPIRE is mainly comprised of two parts: the power package; and the digital sensor package. The power package includes an electromagnetic energy harvester, power processing circuits, and energy storages. The digital sensor package includes sensors, microcontrollers, data storages, and wireless communication devices. The entire embedded system is powered by the included energy harvester, making VAMPIRE a true self-powered sensor node.

A. Energy Harvester

The energy harvester in VAMPIRE extracts energy from electromagnetic coupling formed between the current-carrying wire of an electromechanical device and the electrical system of the sensor node through a magnetic core. Here assumed is that the primary side — the electromechanical device, e.g., a motor — carries an AC sinusoidal current when it is operating. Time-varying magnetic field (H) around the primary wire, generated by the AC sinusoidal current, induces time-varying magnetic flux density (B) according to the B-H curve of the core material. As the Maxwell-Faraday equation states, the time-varying B field induces voltage if the secondary winding exists. At the same time, according to Ampere's law, a current may be induced on the secondary side as well, depending upon the existence of a load. Nonzero secondary voltage and nonzero secondary current at the same time imply that nonzero energy can be harvested and transferred from the primary side to the secondary side without forming an ohmic contact between the two.

This description is identical for the structure of a current transformer, too. The most notable and crucial difference between a current transformer and an electromagnetic energy harvester is that for energy harvesting purposes the magnetic core is intentionally saturated to the full extent every line cycle for maximum energy extraction (or twice in every line cycle considering a rectifier), whereas in normal applications with magnetic cores, such as inductors and transformers, the saturated region of the B-H loop is intentionally avoided because of the importance of the linearity of a magnetic core.

The detailed analysis on magnetic saturation and its importance in the scope of electromagnetic energy harvesting can be referenced at [5] and [6]. The importance of magnetic saturation in energy harvesting can be briefly explained in two ways: first, if the magnetic core is not saturated, the load voltage can be always increased until the core saturates, directly increasing the energy extraction (since it is a current-driven transformer, the harvested current does not change until saturation); second, if the magnetic core is not saturated, the number of turns on the secondary side can be lowered until the core saturates, directly increasing the harvested current (hence energy extraction). An ideal magnetic core for this type of energy harvesting requires three properties: low hysteresis loss, high saturation flux density, and extremely high magnetic permeability [6], [12]. Another important property is the physical size of the core as VAMPIRE is to be enclosed in a small terminal box of the motor. VAMPIRE uses a small toroidal amorphous nanocrystalline core (VAC W380) with the full hysteresis loss of $0.125\,\mathrm{mW}$, saturation flux density of $1.19\,\mathrm{T}$, and the relative initial permeability of approximately $274,027$. The outer and inner diameter of the core is $25\,\mathrm{mm}$ and $16\,\mathrm{mm}$, respectively, and the thickness of the core is $10\,\mathrm{mm}$.

Rectification and power-processing is required on the induced AC current on the secondary side. VAMPIRE uses the transfer window alignment (TWA) method [6] along with active rectification [6], [12] for enhancing energy extraction. The flux-shaping capacitor (FSC) method [6] is not employed as VAMPIRE is designed for a wide range of the primary current levels. The wire gauge of AWG23 is chosen for the secondary side windings, as it can limit the parasitic flux accumulation [13] under 10% up to the primary current of $100\,\mathrm{A_{RMS}}$, which is the maximum design target of VAMPIRE. As will be mentioned shortly, the power required for the nominal operations, including sensing, control, data storage, and the basic wireless communication, is approximately $40\,\mathrm{mW}$. In a conservative estimation, this power requirement can be sustained by having a primary side current of approximately $4.0\,\mathrm{A_{RMS}}$ or higher. The harvested current, rectified and maximized through the TWA method, is then stored into a supercapacitor block, which consists of two supercapacitors in series. The voltage of the supercapacitor block is regulated at $4.0\,\mathrm{V}$ to provide $J = 0.6$ for the TWA method, which gives 90% of the maximally achievable power [6].

When the supercapacitor block is fully charged, the harvested current is then rerouted to the energy buffer, which is a $220\,\mathrm{mAh}$ LiPo battery. The energy buffer is required for supplying power to the entire system during a motor's spin-down event, where magnetic fields do not exist, hence zero energy extraction. The sensor data collected immediately before and after a spin-down event contains rich information regarding the health of the electromechanical system. Note that

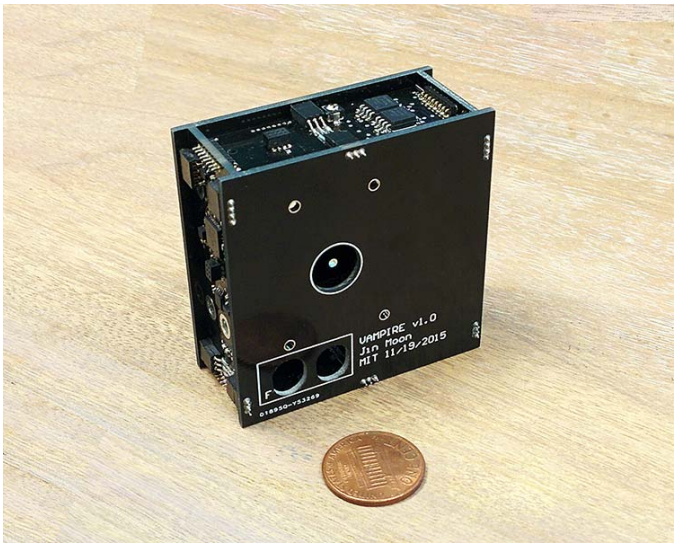

Fig. 2. VAMPIRE Unit Comapred to a US cent coin

as VAMPIRE is a standalone self-powered system, it should be guaranteed that the energy buffer must be utilized such that net positive energy flows into the energy buffer between VAMPIRE operations.

B. Digital Sensor Package

The digital sensor package consists of microcontrollers, a 3-axis accelerometer, a temperature sensor, a back-EMF sensor, data storage devices, a real-time clock, and wireless communication devices. The data storage devices include two Ferroelectric RAMs (FRAM) and one SD card. The wireless communication devices include a Bluetooth Low Energy (BLE) module and a WIFI module. The accelerometer and the back-EMF sensor are sampled at $2\,\mathrm{kHz}$, and the temperature sensor is sampled at $20\,\mathrm{Hz}$. The accelerometer measures the vibration of a motor, from which a relative vibrational energy is inferred. The back-EMF sensor measures the back-EMF voltage appearing across the phase wires of an electromechanical machine when the machine is spinning down. This back-EMF voltage data is used to infer the rotational speed of the machine during the spin-down. Figure 2 illustrates the VAMPIRE unit before installation in the control box of a motor, compared to a US one-cent coin. The physical size is approximately $54.28\,\mathrm{mm} \times 54.28\,\mathrm{mm} \times 23.2\,\mathrm{mm}$.

C. Automated Data Collection

When the sensors are queried, the retrieved data is immediately written to the FRAM block that consists of two 4Mb FRAM modules. This FRAM block allows writing of approximately 100 seconds worth of data samples at $2\,\mathrm{kHz}$. The FRAM block is written in a ring fashion, overwriting the oldest data automatically. If a spin-down event is detected, the time is marked as $t = 0$, and the start point and the end point for this event recording are marked in the FRAM block, according to the pre-specified spin-down window length. In VAMPIRE, $t = -85\,\mathrm{s}$ and $t = +15\,\mathrm{s}$ with reference to the

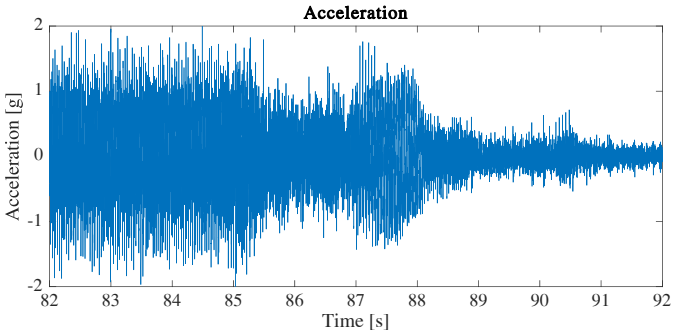

(a) VAMPIRE Acceleration Data

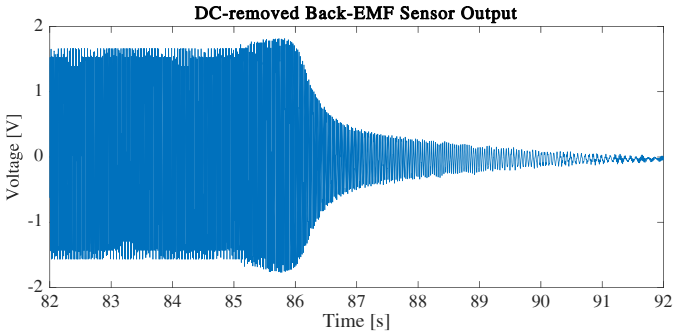

(b) VAMPIRE Back-EMF Data

Fig. 3. Raw time-domain data captured by VAMPIRE during a spin-down event

spin-down detection are the marked in the FRAM block as the start and the end points of this event. Once the end point is reached, which is 15 seconds after the primary side is turned off, the entire FRAM contents are transferred to the SD card in a time-sorted fashion with the aid of the marked locations. The real-time clock is also queried as the file is created in the SD card. The SD card is required in the design because an FRAM module is extremely limited in data storage capacity compared to its physical size. However, FRAM modules are also essential in that the SD card consumes much higher power than an FRAM module for nominal operations. Also, the SD card is not appropriate for constant low latency writings. It necessitates an additional buffer layer to do so, requiring an FRAM or SRAM again. Each recorded spin-down event contains 100 seconds of 3-axis acceleration data and back-EMF data at $2\,\mathrm{kHz}$ in addition to 100 seconds of temperature data at $20\,\mathrm{Hz}$. Each sampled acceleration data is 10 bits per axis. Each sampled back-EMF data is also 10 bits.

After the automated data collection, the entire embedded system goes into an idle mode, supported by the energy buffer. The BLE advertisement is still ongoing during this time such that an external BLE device can make a connection to VAMPIRE. However, to guarantee the net positive energy flow into the energy buffer, the time that VAMPIRE can wait for the BLE connection can be limited. If a user wants to download recorded spin-down raw data files, the WIFI module is activated and the file is transferred through WIFI. Since WIFI is extremely power consuming, the duration which WIFI connection is alive should be actively managed by a user. If

the net positive energy flow policy is violated, VAMPIRE has to charge the energy buffer for a much longer time at the next energy harvesting opportunity.

Figure. 3 illustrates the actual raw data file downloaded from VAMPIRE. The collected vibration data, which is the axis parallel to gravity, is illustrated at the top, and the back-EMF sensor data is illustrated at the bottom. The motor was turned off at the 85 second mark. Since VAMPIRE automatically detects a spin-down event and the raw data file is marked with the spin-down window boundaries, multiple raw data files can be easily analyzed without specifying the spin-down location for each file.

IV. eVTF Generation

The signal-processing method for generating an eVTF from vibration and back-emf voltage data is described in detail in [8]. The important aspects as they relate to the field application are included below.

A. Time-Domain Processing

In VAMPIRE, the back-EMF voltage developed across the phase wires of a motor is capacitively coupled and then amplified through an opamp. This structure inherently introduces a differentiator, which requires an integrator at a later stage for a proper reconstruction of the signal. However, in order to suppress the nominal current consumption of the embedded system, VAMPIRE records the 'differentiated' back-EMF data directly into its data storage, with the intention of digital integration during the signal processing stage. During a software integration, there can be a DC drift due to various environmental reasons, e.g., quantization error, finite sampling frequency, etc. This can be effectively removed by applying a digital high-pass filter. In this analysis, the 4th order high-pass Butterworth filter with the cut-off frequency of 6 Hz is applied. Figure 4 illustrates the raw 'differentiated' back-EMF measurement from VAMPIRE, the software-integrated signal, and the filtered and reconstructed back-EMF voltage measurement, from top to bottom, respectively.

From the back-emf voltage measurement, the electrical-speed profile $\omega_e(t)$ can be estimated using a zero-crossing detection procedure. Here, the k_{th} zero-crossing is identified by a change of sign between two adjacent waveform samples at t_n and t_{n+1}, and its time-location, $t[k]$ estimated based on the zero-value of the linear interpolation of the signal values $V_o(t_n)$ and $V_o(t_{n+1})$. Then, the signal frequency at time instance, $t[k]$, is estimated as,

$$\hat{\omega}_e(t[k]) = \frac{2\pi}{t[k+1] - t[k-1]}. \tag{10}$$

In the discussion above, n represents the sample time-index, and k represents the time indexing of zero-crossings.

From the $\hat{\omega}_e$ estimates, the mechanical speed estimate, $\hat{\omega}_m$, is calculated based on the number of pole-pairs in the machinery. Then, this stream is linearly interpolated to match the sampling rate of the original measurements for calculating the virtual input function, $\Phi_m(t)$, from (4).

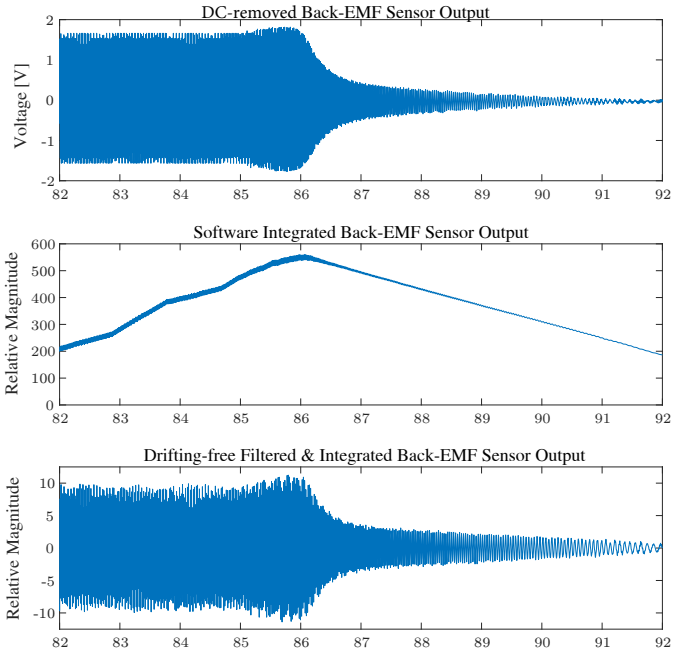

Fig. 4. Back-EMF Raw Data Processing

B. Frequency-Domain Processing

In accordance with (5), the time-domain spin-down signals of Fig. 3 need to be transformed into frequency domain signals. This is done using the Short-time Fourier Transform (STFT). Here, the time-domain waveforms are windowed at a series of time locations during the spin down process, and the Fast Fourier Transform (FFT) is used to process each modified time signal resulting in a time-binned frequency representation of the original signals. For this application, a Hanning window with a width of 1.0 s is used as the mask for the input and output waveforms, and each successive Hanning window overlaps the previous by 90%.

Each resulting frequency spectrum is specific to a short period of time during the spin down process. These spectrums are indexed as $\Phi_{m,i}(j\omega)$ and $A_{m,i}(j\omega)$, respectively, where i denotes the Hanning window index.

To generate the eVTF, maximum envelope excitation and response spectrums are defined as,

$$\Phi_{env}(j\omega) = \max_i \left[\underset{\Phi_{m,i}(j\omega)}{\operatorname{argmax}} |\Phi_{m,i}(j\omega)| \right], \tag{11}$$

and

$$A_{env}(j\omega) = \max_i \left[\underset{A'_{m,i}(j\omega)}{\operatorname{argmax}} |A'_{m,i}(j\omega)| \right], \tag{12}$$

respectively. That is, at a given frequency, these envelopes are defined as equal to the corresponding indexed spectrum with the maximum magnitude at that particular frequency. The eVTF is then determined as,

$$\frac{A_m(j\omega)}{\Phi_m(j\omega)} = \frac{A_{env}(j\omega)}{\Phi_{env}(j\omega)}. \tag{13}$$

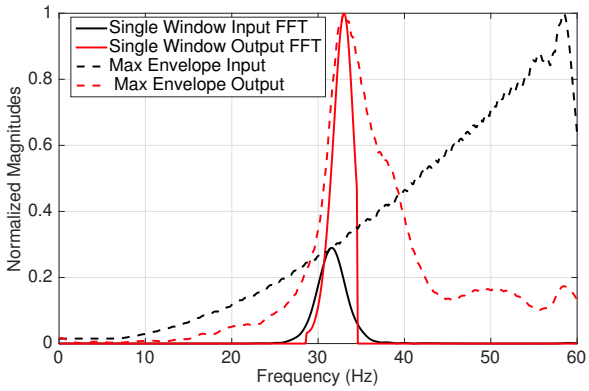

Fig. 5. Fast Fourier Transform of Masked Inputs and Masked Outputs with Envelopes

Generating the eVTF in this manor allows the maximum amount of information gained during the STFT based analysis to be passed on to the eVTF while also ensuring linearity.

Fig. 5 shows a graphical representation of this process. In this figure, the magnitudes shown on the y-axis are normalized to the maximum values of each input and output spectrum series, $\Phi_{m,i}(j\omega)$ and $A_{m,i}(j\omega)$, respectively. The dashed curves represent the STFT envelopes of (11) and (12), while the solid lines represent individual spectrums from a windowed time segment roughly half-way through the spin-down. This particular period also corresponds to the peak resonance in the system. The figure shows that the FFT for the virtual input signal has a maximum at around 31.5 Hz while the resulting FFT for the output vibration signal has a maximum at around 33 Hz. This offset is due to the fact that there is a time delay in the vibrational response to the forcing input.

V. Experiment

A. Experiment Setup

VAMPIRE is installed in a real vibration testing setup with a 3-phase AC motor, as shown in Fig. 6. The bright green cover for motor's terminal box is 3-D printed to provide a secure mount for VAMPIRE, replacing the existing cover. For the same task of generating an eVTF, this retrofit installation of VAMPIRE effectively replaces all the hardware required in [8]: commercial off-the-shelf accelerometers; standalone back-EMF sensors; data acquisition blocks; data storage; wireless network capability; and external power supply and wiring.

One of the three phase wires of the AC motor goes through the center of VAMPIRE for electromagnetic energy harvesting. This wire and one additional phase wire are capacitively coupled to provide a differential voltage input to the back-EMF sensor. Though this figure shows wirings outside the cover for debug and measurement purposes, wirings can be neatly contained inside the box and the front face can be sealed.

The overall electromechanical test structure is depicted in Fig. 7. The 3-phase AC motor takes in 3-phase power input, and spins the load connected to the shaft: the DC motor acting as dynamo and an unloaded AC motor acting as a flywheel.

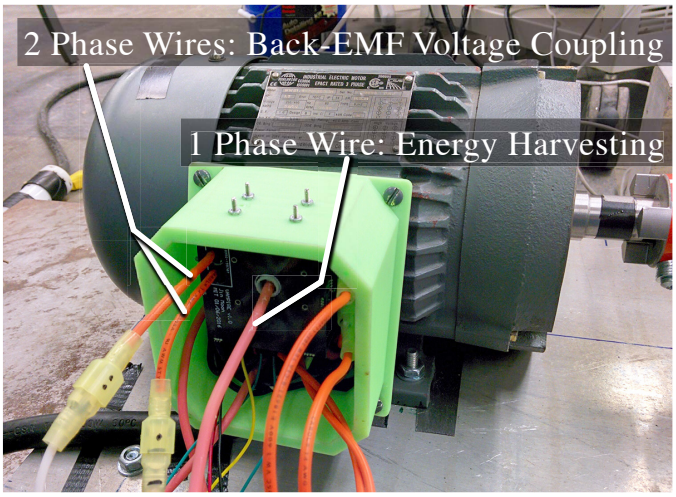

Fig. 6. VAMPIRE Installed in the Control Box of the Motor

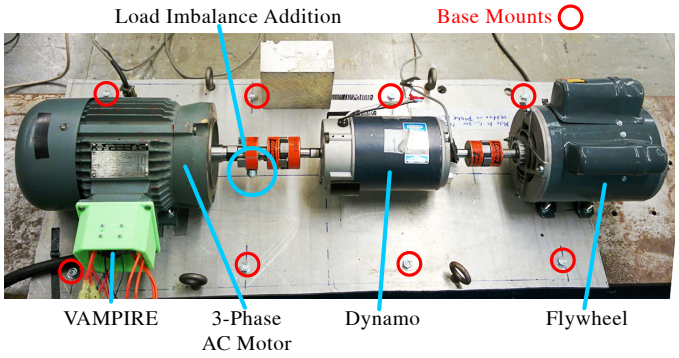

Fig. 7. Test Setup: Electromechanical System under Diagnosis

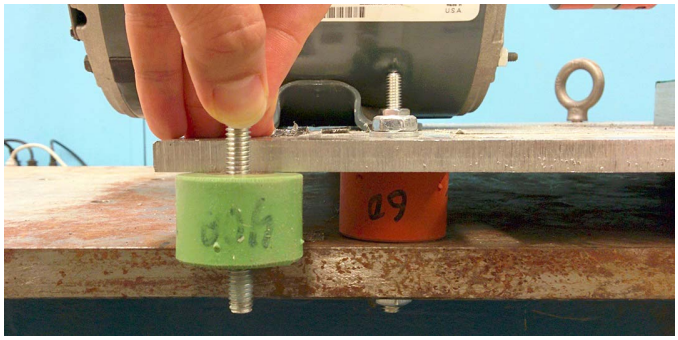

Fig. 8. Test Setup: Mounting Structure

There is an option to add a load imbalance of 17 g to the shaft. The AC motor is rated up to 1.5 hp (1.1 kW), with the steady state revolutions per minute (RPM) of approximately 3,500 at the line frequency of 60 Hz. The electrical connections of the DC motor are left disconnected when the AC motor is powered. This electromechanical test structure is mounted on a thick metal plate that acts as the base, and this base plate sits on a metal box beam with mounts in between as shown in Fig. 8. The mounts can be swapped for different stiffness. The goal of this experiment is to obtain eVTFs under different

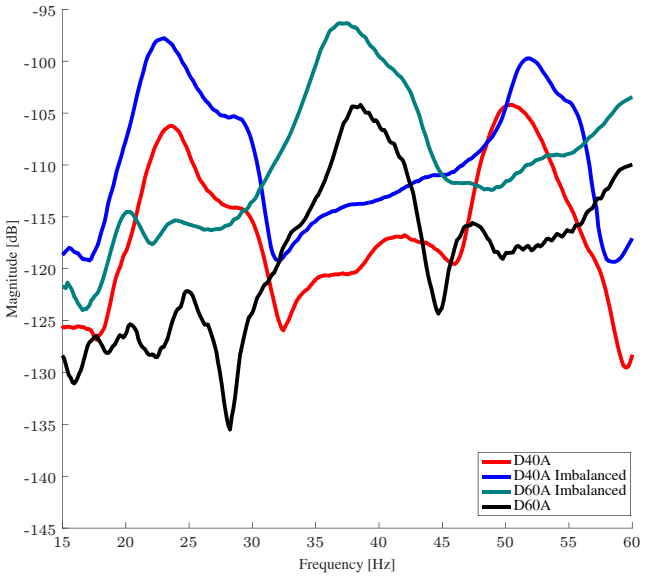

Fig. 9. eVTF Results

mechanical conditions that imitate mechanical failures, with the expectation of clear changes in eVTFs. Two different mounts with durometer of 40A and 60A are tested. At the same time, a load imbalance of 17 g or 0 g (no imbalance) is considered, giving a total of 4 cases. Four data files generated from four spin-down events with four different conditions are downloaded from VAMPIRE, and analyzed with the signal processing method described in the previous section.

B. Results

The experiment result is illustrated in Fig. 9. Consider the red curve, 'D40A', as the base case. When the imbalance is added to the shaft, C in (5) is increased. Since the y-axis is in dB, the increased coefficient results in a vertical shift, as seen in the blue curve, 'D40A Imbalance.' When the D40A mounts are replaced with the D60A mounts (but still with the load imbalance), the increase in the stiffness of the mounts results in different vibration dampening and brings an increase in the mechanical self-resonant frequency. This clearly manifests as a horizontal shift to the right, as seen in the green curve, 'D60A Imbalance.' When the load imbalance is removed from the D60A mounts, the vertical shift in the reverse direction happens as C is decreased, presenting the black curve, 'D60A.'

Therefore, by monitoring changes in eVTFs over time, two separate electromechanical issues can be diagnosed: a change in mount stiffness and a change in load imbalance. A change in stiffness can imply damaged or degraded mounts. A change in load imbalance can imply a damaged load, a changed load profile, or a damaged shaft axle. Heuristics to quantify the shape of an eVTF, e.g., locations of the primary peaks and corresponding magnitudes, slopes at certain regions, etc., can be implemented on a continuous monitoring system that communicates with VAMPIRE, and automatically generate an indication for CBM.

VI. Conclusion

The self-powered embedded system, VAMPIRE, is successfully designed, built, and deployed in a real world environment. The entire embedded system is sustained by the onboard electromagnetic energy harvester. VAMPIRE can be accessed by BLE, and the collected sensor data can be wirelessly downloaded from VAMPIRE through WIFI.

Signal processing methods for generating an eVTF from the raw sensor data are introduced. The eVTFs of four different mechanical conditions are constructed using raw data files experimentally obtained from VAMPIRE, and vertical and horizontal shifts of eVTFs are clearly verified with a change in load imbalance and a change in the mount stiffness, respectively. A change in eVTFs over time can be used as a clear indication for CBM.

VAMPIRE with the correct signal processing ultimately enables easier, nonintrusive, and automated failure prevention and low-cost maintenance for electromechanical systems.

Acknowledgment

The authors would like to thank the Office of Naval Research Structural Acoustics Program and The Grainger Foundation.

References

[1] S. Yang, "A condition-based failure-prediction and processing-scheme for preventive maintenance," *Reliability, IEEE Transactions on*, vol. 52, no. 3, pp. 373–383, Sept 2003.

[2] A. K. Jardine, D. Lin, and D. Banjevic, "A review on machinery diagnostics and prognostics implementing condition-based maintenance," *Mechanical Systems and Signal Processing*, vol. 20, no. 7, pp. 1483 – 1510, 2006.

[3] A. Heng, S. Zhang, A. C. Tan, and J. Mathew, "Rotating machinery prognostics: State of the art, challenges and opportunities," *Mechanical Systems and Signal Processing*, vol. 23, no. 3, pp. 724 – 739, 2009.

[4] Department of Defense, *Condition Based Maintenance Plus DoD Guidebook*, 2007.

[5] J. Moon and S. Leeb, "Analysis model for magnetic energy harvesters," *IEEE Transactions on Power Electronics*, vol. 30, no. 8, pp. 4302–4311, Aug 2015.

[6] J. Moon and S. B. Leeb, "Power electronic circuits for magnetic energy harvesters," *IEEE Transactions on Power Electronics*, vol. 31, no. 1, pp. 270–279, Jan 2016.

[7] J. Moon, J. Donnal, J. Paris, and S. B. Leeb, "Vampire: A magnetically self-powered sensor node capable of wireless transmission," in *Applied Power Electronics Conference and Exposition (APEC), 2013 Twenty-Eighth Annual IEEE*, March 2013, pp. 3151–3159.

[8] R. Zachar, P. Lindahl, J. Donnal, W. Cotta, C. Schantz, and S. B. Leeb, "Utilizing spin-down transients for vibration-based diagnostics of resiliently mounted machines," *IEEE Transactions on Instrumentation and Measurement*, vol. 65, no. 7, pp. 1641–1650, July 2016.

[9] Z. Tang, P. Pillay, and A. Omekanda, "Vibration prediction in switched reluctance motors with transfer function identification from shaker and force hammer tests," *Industry Applications, IEEE Transactions on*, vol. 39, no. 4, pp. 978–985, July 2003.

[10] L. L. Beranek and I. L. Vér, Eds., *Noise and vibration control engineering: principles and applications*. Wiley, 1992.

[11] C. J. Schantz, "Methods for non-intrusive sensing and system monitoring," Ph.D. dissertation, Massachusetts Institute of Technology, 2014.

[12] J. Moon and S. B. Leeb, "Enhancement on energy extraction from magnetic energy harvesters," in *2015 IEEE Energy Conversion Congress and Exposition (ECCE)*, Sept 2015, pp. 427–433.

[13] J. Moon and S. B. Leeb, "Power loss analysis with high primary current in magnetic energy harvesters," in *2015 IEEE 16th Workshop on Control and Modeling for Power Electronics (COMPEL)*, July 2015, pp. 1–8.